2024 IEEE/RSJ International Conference on Intelligent Robots and Systems (IROS)
October 14-18, 2024. Abu Dhabi, UAE

Modeling of Hydraulic Soft Hand with Rubber Sheet Reservoir and Evaluation of its Grasping Flexibility and Control

Kyosuke Ishibashi[1], Hiroki Ishikawa[1], Osamu Azami[1] and Ko Yamamoto[1]

***Abstract*— In situations where robots work alongside humans, they must be capable of responding flexibly to unexpected external forces. To address this challenge, researchers have conducted numerous studies on soft robotics. However, most of the soft hands studied so far are powered by pneumatic pressure and can only exert pressure up to a several hundred kPa, resulting in low output. To solve this problem, we have developed a hydraulic soft hand in our previous research. In this paper, we derive the relationship between driving pressure, bending angle, and grasping force of a soft hand with a reservoir to evaluate the effect of a rubber sheet reservoir. Additionally, we experimentally show that the soft hand provides grasping flexibility when angle control is applied using the model proposed in this paper.**

I. Introduction

The integration of robots in various industries, including logistics, construction, and agriculture, has become necessary due to the scarcity of available workers. In situations where robots work alongside humans, they must be capable of responding flexibly to unexpected external forces, such as collisions with people or objects, to ensure safety. To address this challenge, researchers have conducted numerous studies on soft robotics, using soft materials for certain robot components [1], [2]. Soft hands capable of grasping vegetables, processed foods, and objects with varying and unknown shapes have been developed [3], [4]. However, most of the soft hands studied so far are powered by pneumatic pressure and mainly have two problems; The first limitation is that it can only generate a maximum pressure of several hundred kPa, resulting in low output. The second limitation is that it requires a large external compressor, which is inefficient because it needs to release high-pressure air each time the fingers are deformed.

For the first issue, Yap et al. [5] and Wang et al. [6] have developed pneumatically driven soft hands capable of grasping objects weighing up to 5 kg and 10 kg, respectively. However, they reported that the grasping force was decreased when the diameter of the object was larger, indicating a challenge in grasping heavy objects with large diameters.

Therefore, this study focuses on a hydraulic-driven soft hand that can grasp heavier objects due to the ability to apply pressure in the order of several MPa. Additionally, by attaching a reservoir to the hand to store oil, the charge pressure can be effectively used, allowing the fingers to bend at a lower differential pressure to achieve the same target angle. Hagiwara et al. [7] developed a hydraulically driven soft hand capable of grasping objects weighing up to 5 kg with two fingers. We have developed a hydraulically driven soft hand for transporting heavy vegetables in a food factory [8], [9]. The hand was able to grasp cabbages of varying shapes and postures that were stacked in baskets.

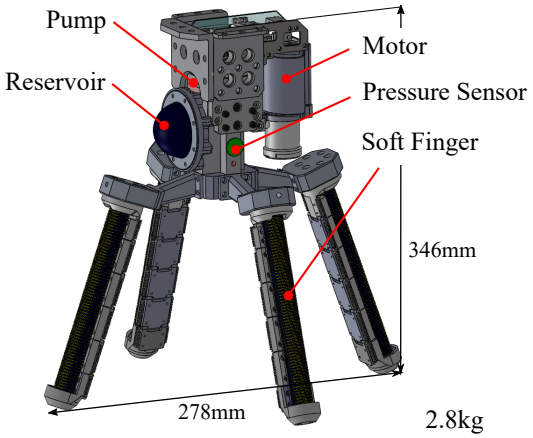

Fig. 1. Four-fingered hydraulic soft robot hand

This paper presents an analytical model to consider the effect of a reservoir composed of rubber sheets on the hand. This study analyzed the relationship between driving pressure, bending angle of the fingers, and grasping force for a soft hand with a reservoir inside. Furthermore, using the obtained model, we controlled the bending angle of the fingers in two degrees of freedom and evaluated the grasping flexibility of the soft hand using the same flow path for each finger when an external force was applied.

II. Hydraulic Soft Hand

A. Structure of hydraulic soft hand

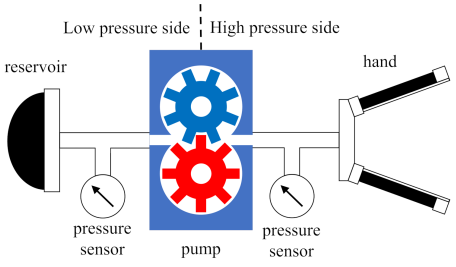

Fig. 2. Simple diagram of the robotic soft hand

[1]Kyosuke Ishibashi, Hiroki Ishikawa, Osamu Azami and Ko Yamamoto are with Department of Mechano-informatics, The University of Tokyo 7-3-1 Hongo, Bunkyo-ku, Tokyo 113-8656, Japan {ishibashi-kyosuke, hiroki-ishikawa, azami-osamu, yamamoto.ko}@ynl.t.u-tokyo.ac.jp

Fig. 1 shows the soft hand developed in this study. It is 278 mm wide, 346 mm high, and weighs approximately 2.8 kg, including hydraulic pump and electric motor. The hand is composed of soft fingers, pressure sensors, a reservoir for storing oil, a hydraulic pump, and a motor for driving the pump. The fingers are mounted diagonally outward from the hand at a 20-degree angle. As illustrated in Fig. 2, soft fingers are attached to the flow path on the high pressure side of the hydraulic pump and a reservoir is attached to the flow path on the low pressure side. The pump generates a differential pressure and sends oil from the reservoir to the soft fingers, causing the fingers to bend. The pump was developed by Komagata et al. [10].

B. Structure of Fiber Reinforced Soft Finger

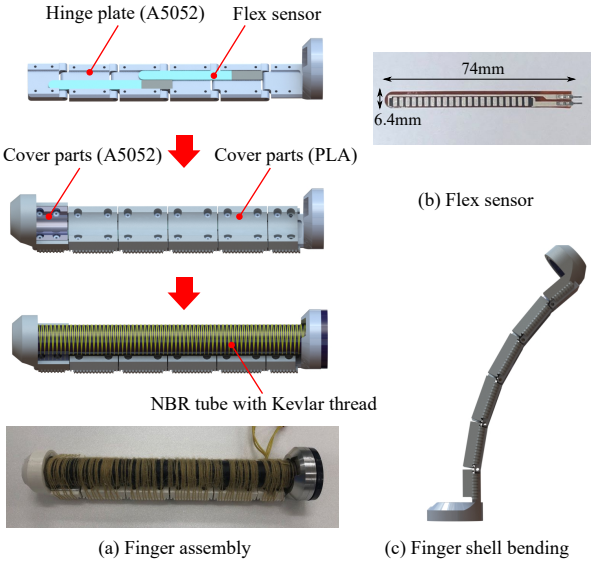

Fig. 3. Fabricated soft finger. (a) Structure of soft finger, (b) Resistive flexible sensor, (c) Image of finger shell bending.

Fig. 3 shows the developed fiber-reinforced soft finger [8], [9]. Fiber-reinforced soft fingers utilize the expansion of soft materials under pressure and deform only in a certain direction by embedding inelastic materials [11], [12]. The rubber parts of the fingers are made of nitrile rubber (NBR) with a Shore A hardness of 70, and are cylindrical in shape with a length of 180 mm. Kevlar threads are wrapped around the fingers to prevent radial expansion. The outer shell of the fingers is made of A7075 metal parts and PLA 3D printer parts, and has a hinge structure to prevent the fingers from twisting when grasping objects. The fabricated fingers were confirmed to be capable of withstanding high pressure of 2.0 MPa through the use of finite element (FEM) simulation. Furthermore, it was demonstrated that the fingers could grasp an object weighing 20 kg when the aforementioned pressure was applied.

III. Modeling and Sensing of Soft Hand

A. Analytical Modeling of Soft Hand

Then, we formulate a mathematical model to represent the relationship among the driving pressure, bending angle of a finger, and grasping force assuming a target object. Previously, Renda et al. [13] proposed a PCS model dividing a flexible rod structure into a finite number of segments with a constant strain and derived its kinematics and dynamics. Polygerinos et al. [14], [15] modeled fiber-reinforced soft fingers, assuming constant curvature, while Mustaza et al. [16] developed a manipulator with fiber-constrained actuators and used Lagrange's equations for dynamic modeling. Sedal et al. [17] derived equations for fiber-constrained soft actuators, relating various mechanical parameters under static conditions using continuum mechanics. However, these studies focused on modelling of a soft finger itself without considering the entire hand system. In this paper, we formulate a mathematical model including soft fingers and the reservoir made of a hyperelastic rubber sheet, and show that the elasticity of the reservoir contributes to an efficient actuation.

First, we consider a geometric model of a finger shown in Fig. 4. Table I summarizes the definition of each parameter. From the virtual work principle, the virtual work by the

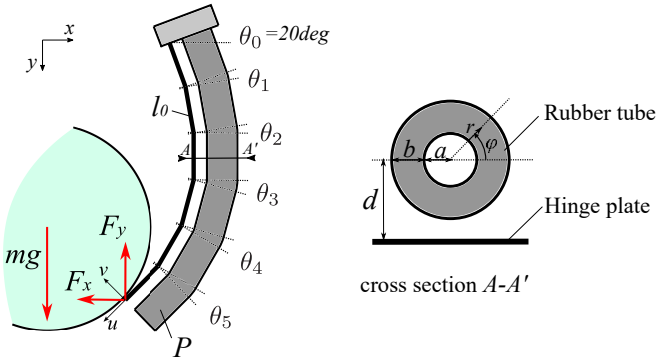

Fig. 4. Model of developed soft hand with rubber sheet reservoir.

pressure P and grasping force (F_x, F_y) is equal to the variations of the strain energies in fingers ΔW_f and in the reservoir sheet ΔW_r, which is represented as

$$P\Delta Q + n(F_x\Delta x + F_y\Delta y) = n\Delta W_f + \Delta W_r \quad (1)$$

The first term on the left-hand side is the virtual work produced by the hydraulic pump, and ΔQ represents the flow rate due to the change in θ. The second and third terms are the work produced by the grasping force, where Δx and Δy represent the virtual displacement in the position of the finger tip, respectively. The first and second terms, ΔW_f and ΔW_r, on the right-hand side are the variations of the strain energies in the finger tube and reservoir sheet, respectively. The details are summarized as follows:

1) Virtual work by hydraulic pump: The virtual work by the hydraulic pump is given by $P\Delta Q$, where Q is amount of internal volume of soft fingers. Assuming that a finger consists of a simple cylinder shape as shown in Fig. 4, Q is calculated as

$$Q = na^2\pi(l_0 + d\theta) \quad (2)$$

$$\theta := \sum_i \theta_i \quad (3)$$

TABLE I

PARAMETERS AND SYMBOLS OF FINGER MODEL.

Param	Description	Value
$\hat{\theta}_0$	Inclination of the base link of the finger	20deg
l_0	Initial length of the finger	180mm
a	Internal diameter of the rubber tube	4mm
b	Thickness of the rubber tube	5mm
d	Distance between hinge plate and rubber tube	15mm
R	Radius of reservoir sheet	24mm
w	Thickness of reservoir sheet	1mm
V_0	Initial volume of oil stored in reservoir	17.8cm^3
n	The number of finger attached to the hand	4
n_s	The number of hinge joint in a finger	5
μ_{sf}	Initial shear modulus of rubber tube (finger)	1.15MPa
μ_{sr}	Initial shear modulus of rubber sheet (reservoir)	1.15MPa

Symbol	Description
P	Pressure of the inner side of the finger
F_x, F_y	Force applied to the tip of the finger
$\hat{\boldsymbol{\theta}} = (\hat{\theta}_1, \cdots, \hat{\theta}_5)^T$	Bend angles between the hinge plate
$\theta = \Sigma\hat{\theta}_i$	Bend angle of finger
m	Mass of the grasping object

Therefore, the virtual work $P\Delta Q$ is calculated as

$$P\Delta Q = Pna^2\pi d\Delta\theta \tag{4}$$

where $\Delta\theta$ is the variation of θ.

2) Variation in strain energy of a finger: Next, we consider the change in strain energy ΔW_f of a nitrile rubber tube. The strain energy W_f of a finger is calculated based on the Neo-Hookean model [18] as

$$W_f = \int \frac{\mu_{sf}}{2}(I_1 - 3)dV \tag{5}$$

where I_1 is the first invariant of deviation strain, represented using the axial, radial and circumferential deformation rates $\lambda_1, \lambda_2, \lambda_3$ as

$$I_1 = \lambda_1^2 + \lambda_2^2 + \lambda_3^2. \tag{6}$$

In this study, $\lambda_2 = 1$ is satisfied because the radial direction is constrained by Kevlar threads. Also, $\lambda_1\lambda_2\lambda_3 = 1$ is satisfied because NBR is an incompressible material. Therefore, letting $\lambda_f = \lambda_1$ denote an alias of λ_1, the values of λ_1, λ_2 and λ_3 are summarized as

$$\lambda_1 = \lambda_f,\ \lambda_2 = 1,\ \lambda_3 = \frac{1}{\lambda_f} \tag{7}$$

Considering a polar coordinate r and ϕ in the cross section A-A' shown in Fig. 4, λ_f is calculated as

$$\lambda_f = \frac{l_0 + \{d + (a+r)\sin\phi\}\theta}{l_0} \tag{8}$$

From (5)-(8), we can represent ΔW_f as

$$\Delta W_f = \mu_{sf}\zeta_f(\theta)\Delta\theta \tag{9}$$

$$\zeta_f(\theta) := \int_0^{2\pi}\int_0^b (\lambda_f - \frac{1}{\lambda_f^3})\frac{d\lambda_f}{d\theta}\cdot l_0(a+r)drd\phi \tag{10}$$

3) Variation in strain energy of the reservoir sheet: The strain energy in the reservoir sheet W_r can be expressed as

$$W_r = \int \frac{\mu_{sr}}{2}(I_1 - 3)dV \tag{11}$$

in a manner similar to (5). Because the rubber sheet is subject to biaxial tensile deformation, the values of λ_1, λ_2 and λ_3 are given as

$$\lambda_1 = \lambda_2 = \lambda_r, \lambda_3 = \frac{1}{\lambda_r^2} \tag{12}$$

where λ_r is an alias of λ_1 or λ_2.

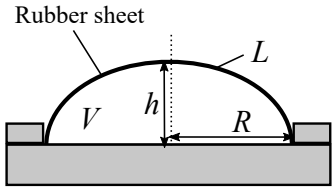

Fig. 5. Model of the reservoir made of rubber sheet.

Fig. 5 shows a schematic diagram of the reservoir. Assuming that the rubber sheet deforms into an ellipse, the circumference L of the ellipse can be written from Ramanujan's approximation [19] as

$$2L(h) = \pi(3(R+h) - \sqrt{(R+3h)(h+3R)}) \tag{13}$$

where R and h are the radius and height of the reservoir, calculated as follows:

$$h = \frac{3}{2\pi R^2}V \tag{14}$$

$$V = V_0 - a^2\pi dn\theta \tag{15}$$

Then, λ_r can be written as

$$\lambda_r = \frac{L(h)}{2R} \tag{16}$$

From (11)-(15), we can calculate ΔW_r as

$$\Delta W_r = \mu_s\zeta_r(\theta)\Delta\theta \tag{17}$$

$$\zeta_r(\theta) := 2(\lambda_r - \frac{1}{\lambda_r^5})\frac{d\lambda_r}{d\theta}\cdot\pi R^2 t \tag{18}$$

4) Virtual work by grasping force: We define $\Delta\boldsymbol{\theta}$ as a vector storing the virtual displacements of joint angles as

$$\Delta\boldsymbol{\theta} = \begin{bmatrix}\Delta\theta_1 & \cdots & \Delta\theta_{n_s}\end{bmatrix}^T. \tag{19}$$

We can write the relationship between the virtual displacement of the finger tip and $\Delta\boldsymbol{\theta}$ as

$$\begin{bmatrix}\Delta x \\ \Delta y\end{bmatrix} = \begin{bmatrix}\boldsymbol{J}_x \\ \boldsymbol{J}_y\end{bmatrix}\Delta\boldsymbol{\theta} \tag{20}$$

where $\boldsymbol{J}_x$ and $\boldsymbol{J}_y$ are the Jacobian matrices.

In general, $\Delta\boldsymbol{\theta}$ is not uniquely determined when given a displacement of the total bending angle $\Delta\theta$. Hence, we represent $\Delta\boldsymbol{\theta}$ using a weighting coefficient vector $\boldsymbol{w}$ as

$$\Delta\boldsymbol{\theta} = \boldsymbol{w}\Delta\theta \tag{21}$$

$$\boldsymbol{w} = \begin{bmatrix} w_1 & \cdots & w_{n_s} \end{bmatrix} \tag{22}$$

Note that $w_1, \cdots, w_{n_s}$ satisfy the following equation.

$$\sum_{i=1}^{n_s} w_i = 1 \tag{23}$$

5) Total virtual work relationship and grasping condition: We assume that the target object is uniformly supported by all fingers, and F_y is given by

$$F_y = \frac{mg}{n} \tag{24}$$

Substituting (4), (9), (17), (20), (21) into (1) and eliminating $\Delta\theta$ yields the following relation for P, θ, F_x, m.

$$Pna^2\pi d + nF_x\boldsymbol{J}_x\boldsymbol{w} + mg\boldsymbol{J}_y\boldsymbol{w} = n\mu_{sf}\zeta_f(\theta) + \mu_{sr}\zeta_r(\theta) \tag{25}$$

B. Relationship between pressure and bend angle

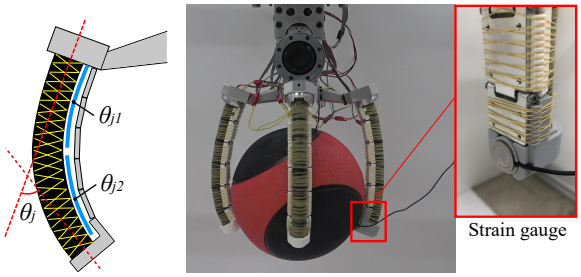

(a) (b)

Fig. 6. Sensors used to measure the state of the fingers. (a) Measurement of bending angles with flex sensors. (b) Gripping force measurement with strain gauge.

To evaluate the obtained model, we attached a strain gauge at the tip of one of the fingers as shown in Fig.6 to measure the contact force. Let θ_j denote the total bending angle of a finger j, which can be obtained as the sum of the measured values by the two bending sensors, θ_{j1} and θ_{j2} as

$$\theta_j = \theta_{j1} + \theta_{j2} \quad (j = 1, 2, 3, 4) \tag{26}$$

First, using the formula (25), we evaluate the relationship between driving pressure and bend angle of the fingers when the hand is not grasping an object. With zero grasping force, the second and third terms in the LHS of (25) become zero, simplifying the relationship to

$$P = f(\theta) = \frac{1}{na^2\pi d}(n\mu_{sf}\zeta_f(\theta) + \mu_{sr}\zeta_r(\theta)) \tag{27}$$

The obtained (27) is shown in Fig. 7 as a solid line. Measured bend angles of the four fingers, $\theta_j (j = 1, 2, 3, 4)$, are shown as circles in Fig. 7. The driving pressure was increased from 0 MPa to 0.8 MPa in 0.1 MPa steps. Here, μ_{sf} and μ_{sr} are set to 1.15 MPa: the physical properties of nitrile rubber with a Shore A hardness of 70. The initial reservoir capacity V_0 is set to 1.78×10^4 mm^3, which has the least squares error between the model and the measured values. The RMSE between the model and measurements was 2.8 degrees.

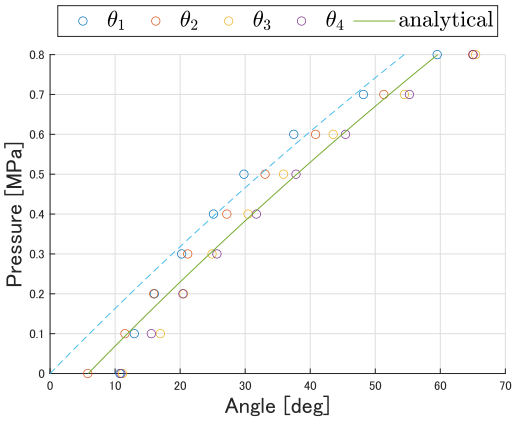

Fig. 7. Relationship between pressure and bend angle of soft finger.

To examine the effect of a rubber sheet reservoir on the hand, we consider the case where the hand has no reservoir. In this case, the equation between the pressure and the bend angle of the fingers becomes

$$P = \frac{\mu_{sf}}{a^2\pi d}\zeta_f(\theta) \tag{28}$$

Equation (28) is represented by the dotted line in Fig. 7. The graph illustrates that the finger can be bent at 0.1 MPa lower pressure when the hand has a reservoir. This is due to the fact that the strain energy of the reservoir can be utilized to bend the fingers.

C. Relationship between pressure, bend angle and grasping force

Next, we evaluate the obtained model by measuring the bending angle θ of the finger and the normal grasping force F_v applied vertically to the fingers. F_v can be expressed as

$$F_v = F_x\cos(\theta - \theta_0) + F_y\sin(\theta - \theta_0) \tag{29}$$

We tested two types of weights: one weighing 2 kg and 180 mm in diameter, and the other weighing 6 kg and 240 mm in diameter. During this experiment, we applied 0.6-0.9 MPa and 1.1-1.4 MPa to grasp the objects, respectively. In (25), the external force term includes a value, $\boldsymbol{w}$, that varies depending on the shape and size of the grasping object. This value was determined in this study based on FEM simulation results. For a 180 mm diameter object, $\boldsymbol{w} = (-0.13, 0.0, 0.67, 0.33, 0.53)^T$ was used, and for a 240 mm diameter object, $\boldsymbol{w} = (-0.2, 0.0, 0.1, 0.3, 0.8)^T$. The results of the measurements for θ and F_v are presented as circles in Fig. 8, while the calculation results of (25) are shown as solid lines in the same figure. The estimation error for the gripping force F_v was 0.22 kgf and 0.39 kgf, respectively. The data points at $F_v = 0$ kgf indicates that the grasped object fell during the experiment.

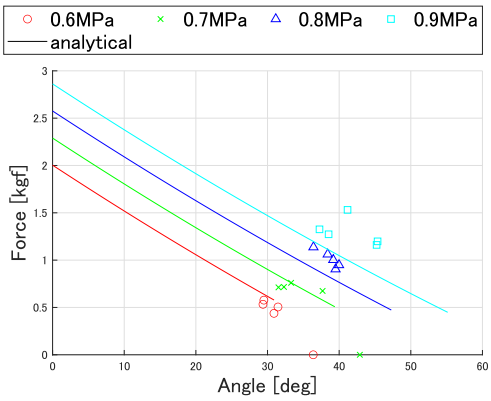

(a) 2kg weight object

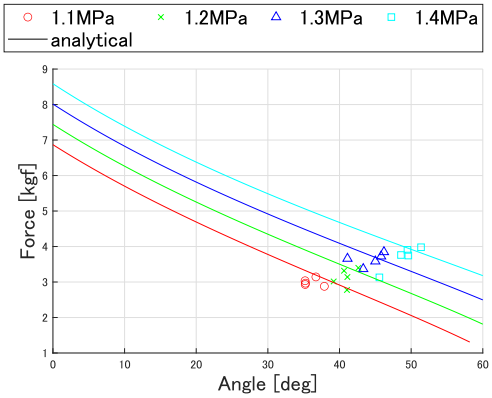

(b) 6kg weight object

Fig. 8. Relationship between finger angle and grasping force in certain pressure.

IV. Finger Control Experiment

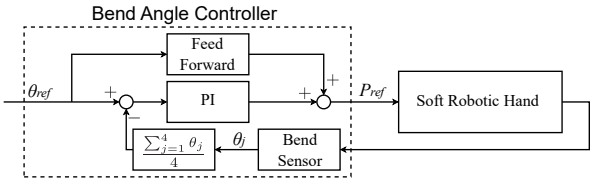

Fig. 9. Two-degree-of-freedom control of the bending angle of the fingers using the relationship between θ and P obtained by (27).

Finally, we conduct an experiment to control the angles of the fingers. We controlled the average angle of fingers to follow reference angle since all fingers are controlled by the single pump. Using the relationship between θ and P obtained by (27), we perform 2-DOF control as shown in Fig. 9. The reference value of the pressure is given as

$$P_{ref} = f(\theta_{ref}) + K_p\theta_e + K_i \int \theta_e dt \tag{30}$$

$$\theta_e = \theta_{ref} - \frac{1}{n}\sum_{j=0}^{n}\theta_j \tag{31}$$

When a reference value of the bending angle θ_{ref} is given, the feedforward term is calculated as $f(\theta_{ref})$ defined by (27). The feedback term is calculated by a PI control of the bending angle error θ_e, defined by (31).

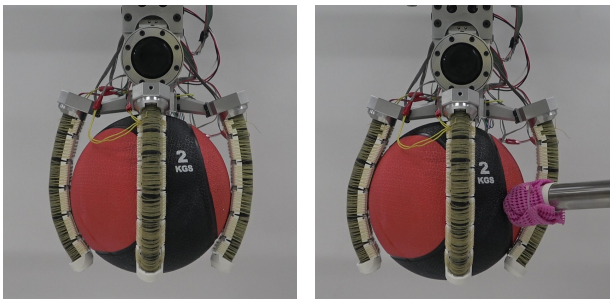

(a) Grasping 2kg weight object (b) Apply external force

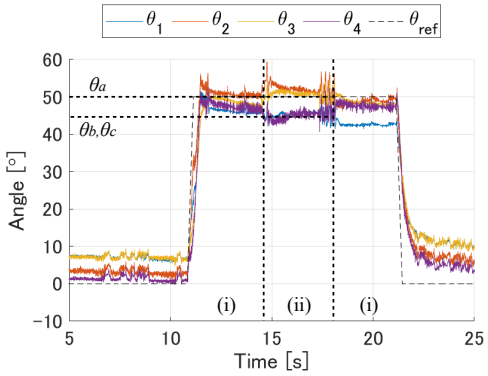

(c) Finger angle graph

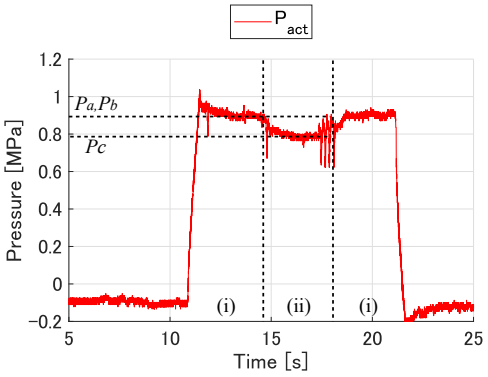

(d) Pressure graph

Fig. 10. Experiment of grasping a 2 kg object by controlling the average bending angle of the four fingers to 50 degrees.

Fig. 10 (a) shows an experiment of grasping a 2 kg object by the closed-loop control with $\theta_{ref} = 50$ degrees. To validate the robustness, after about 5 seconds from the beginning of grasping, we applied an external force to the object, as shown in Fig. 10 (b). The bending angle of each finger is shown in Fig. 10 (c), and the driving pressure is shown in Fig. 10 (d). First, focusing on the state (i) before the external force is applied, we can see that the average value of the fingers can be controlled to about 50 degrees. Next, focusing on state (ii) where external force is applied, we can see that the driving pressure is lower than in state (i). From this result, we can discuss the grasping flexibility of the hand in response to external force when angle control

is applied.

1) Evaluation of Flexibility to External Force: In general, a closed-loop control usually makes a finger more stiff, loosing a flexibility. From the experimental result, we discuss how much flexibility can be achieved by the aforementioned closed-loop control, comparing the grasping force in the following three conditions.

A) Grasping force under the closed-loop control and without any external force. This value is estimated from the values of the pressure P_a and angle θ_a in the period (i) in Fig. 10 (c)
B) Grasping force under the closed-loop control and with an external force applied. This value is estimated from the values of the pressure P_b and angle θ_b in the period (ii) in Fig. 10 (c).
C) Grasping force under the pressure control and with an external force applied. This value is estimated from the value of the angle θ_c in the period (ii) in Fig. 10 (c), assuming that the pressure value P_c is the same with that in the period (i) because the pressure control would keep the pressure value to be constant.

Table II shows the estimated grasping force in each condition. The estimated values for Condition 1, 2 and 3 are 0.61, 0.53 and 0.82 kgf, respectively. Namely, the grasping force against in Condition 2 (closed-loop control) is 0.29 kgf lower than that in Condition 3, which implies that Condition 2 has higher flexibility against the external force. This is different from a general properties of the closed-loop and pressure control — the former achieves stiffness, and the latter achieves flexibility.

TABLE II
DIFFERENCE IN GRASPING FORCE ACCORDING TO CONTROL METHODS.

State	Pressure	Angle	Force
(a) No external force applied to object	0.89MPa	50deg	0.61kgf
(b) External force with pressure control	0.89MPa	45deg	0.82kgf
(c) External force with angle control	0.79MPa	45deg	0.53kgf

V. CONCLUSION

1) The driving pressure, bending angle, and grasping force of a soft hand with a reservoir were derived using the principle of virtual work. The estimated errors of the grasping force were 0.22 kgf and 0.39 kgf for 2 kg and 6 kg objects, respectively. The reservoir, made of a rubber sheet, allows the fingers to bend at a low differential pressure.
2) By controlling the bending angle of the fingers in two degrees of freedom, the study demonstrated the ability to reach the target angle of 50 degrees when grasping a 2 kg object.
3) The soft hand, with the same flow path for each finger, exhibited a reaction force 0.29 kgf lower when the fingers were angle-controlled rather than pressure-controlled. Unlike rigid robot hands, the soft hand is experimentally shown to provide grasping flexibility when angle control is applied.

ACKNOWLEDGMENT

This research was supported by the National Agriculture, Forestry and Fisheries Research Organization's International Competitiveness Enhancement Technology Development Project "Development of Agricultural Work Automation Technology Utilizing Robot Arms Suitable for Agricultural Products" (Research Leader: Takanori Fukao).

REFERENCES

[1] D. Rus and M. T. Tolley, "Design, fabrication and control of soft robots," *Nature*, vol. 521, no. 7553, pp. 467–475, 2015.
[2] J. Shintake *et al.*, "Soft robotic grippers," *Advanced materials*, vol. 30, no. 29, p. 1707035, 2018.
[3] V. Ho and S. Hirai, "Design and analysis of a soft-fingered hand with contact feedback," *IEEE Robotics and Automation Letters*, vol. 2, no. 2, pp. 491–498, 2016.
[4] Y. Yamanaka *et al.*, "Development of a food handling soft robot hand considering a high-speed pick-and-place task," in *2020 IEEE/SICE International Symposium on System Integration (SII)*. IEEE, 2020, pp. 87–92.
[5] H. K. Yap *et al.*, "High-force soft printable pneumatics for soft robotic applications," *Soft Robotics*, vol. 3, no. 3, pp. 144–158, 2016.
[6] D. Wang *et al.*, "A pneumatic novel combined soft robotic gripper with high load capacity and large grasping range," in *Actuators*, vol. 11, no. 1. MDPI, 2021, p. 3.
[7] K. Hagiwara *et al.*, "On high stiffness of soft robots for compatibility of deformation and function," *Advanced Robotics*, vol. 36, no. 19, pp. 995–1010, 2022.
[8] O. Azami *et al.*, "Development of hydraulically-driven soft hand for handling heavy vegetables and its experimental evaluation," in *2023 IEEE International Conference on Robotics and Automation (ICRA)*. IEEE, 2023, pp. 2577–2583.
[9] K. Ishibashi *et al.*, "Compact water pump and its application to self-contained soft robot hand for vegetable factory," *Advanced Robotics*, vol. 37, no. 15, pp. 970–986, 2023.
[10] M. Komagata *et al.*, "Design and development of compact ceramics reinforced pump with low internal leakage for electro-hydrostatic actuated robots," in *Advances in Mechanism and Machine Science: Proceedings of the 15th IFToMM World Congress on Mechanism and Machine Science 15*, 2019, pp. 2439–2448.
[11] K. Suzumori *et al.*, "Flexible microactuator for miniature robots," in *[1991] Proceedings. IEEE Micro Electro Mechanical Systems*. IEEE, 1991, pp. 204–209.
[12] R. Deimel and O. Brock, "A novel type of compliant and underactuated robotic hand for dexterous grasping," *The International Journal of Robotics Research*, vol. 35, no. 1-3, pp. 161–185, 2016.
[13] F. Renda *et al.*, "Discrete cosserat approach for multisection soft manipulator dynamics," *IEEE Transactions on Robotics*, vol. 34, no. 6, pp. 1518–1533, 2018.
[14] P. Polygerinos *et al.*, "Modeling of soft fiber-reinforced bending actuators," *IEEE Transactions on Robotics*, vol. 31, no. 3, pp. 778–789, 2015.
[15] Z. Wang *et al.*, "Interaction forces of soft fiber reinforced bending actuators," *IEEE/ASME Transactions on Mechatronics*, vol. 22, no. 2, pp. 717–727, 2016.
[16] S. M. Mustaza *et al.*, "Dynamic modeling of fiber-reinforced soft manipulator: A visco-hyperelastic material-based continuum mechanics approach," *Soft Robotics*, vol. 6, no. 3, pp. 305–317, 2019.
[17] A. Sedal *et al.*, "A continuum model for fiber-reinforced soft robot actuators," *Journal of Mechanisms and Robotics*, vol. 10, no. 2, p. 024501, 2018.
[18] M. S. Xavier *et al.*, "Finite element modeling of soft fluidic actuators: Overview and recent developments," *Advanced Intelligent Systems*, vol. 3, no. 2, p. 2000187, 2021.
[19] R. W. Barnard *et al.*, "Inequalities for the perimeter of an ellipse," *Journal of mathematical analysis and applications*, vol. 260, no. 2, pp. 295–306, 2001.